International Journal of Hydrogen Energy 78 (2024) 1429–1437

Contents lists available at ScienceDirect

International Journal of Hydrogen Energy

journal homepage: www.elsevier.com/locate/he

Demonstrating the applicability of Raman spectroscopy for the characterization of hydrogen loading of bicyclic liquid organic hydrogen carriers (LOHCs) under process-relevant conditions

Julius H. Jander [a], Michael H. Rausch [a], Peter Wasserscheid [b,c,d], Andreas P. Fröba [a,*]

[a] Institute of Advanced Optical Technologies – Thermophysical Properties (AOT-TP), Department of Chemical and Biological Engineering (CBI) and Erlangen Graduate School in Advanced Optical Technologies (SAOT), Friedrich-Alexander-Universität Erlangen-Nürnberg (FAU), Paul-Gordan-Straße 8, 91052, Erlangen, Germany
[b] Institute of Chemical Reaction Engineering (CRT), Department of Chemical and Biological Engineering (CBI), Friedrich-Alexander-Universität Erlangen-Nürnberg (FAU), Egerlandstraße 3, 91058, Erlangen, Germany
[c] Forschungszentrum Jülich GmbH, Helmholtz Institute Erlangen-Nürnberg for Renewable Energy (IEK-11), Cauerstraße 1, 91058, Erlangen, Germany
[d] Forschungszentrum Jülich GmbH, Institute for a Sustainable Hydrogen Economy, Am Brainergy Park 4, 52428, Jülich, Germany

ARTICLE INFO

Handling Editor: Ramazan Solmaz

Keywords:
LOHC
Diphenylmethane
Benzyltoluene
Raman spectroscopy
Degree of hydrogenation
Hydrogen storage

ABSTRACT

During hydrogenation and dehydrogenation reactions of liquid organic hydrogen carriers (LOHC), their thermophysical properties change significantly as a function of the degree of hydrogenation (*DoH*). Compared with conventional techniques, Raman spectroscopy offers a contactless methodology for online process monitoring without the need of sampling. This work demonstrates the application of Raman spectroscopy for the determination of the *DoH* under process-relevant conditions for LOHC systems based on diphenylmethane (DPM) and benzyltoluene (BT) up to 473 K. For the DPM-based system, a previous study is extended by examining the influence of process-like disturbances. For the BT-based system, a novel approach using indirect hard modeling of the unpolarized Raman spectra is applied, which results in strongly reduced uncertainties and insensitivity towards process-like disturbances, e.g. reaction by-products. For a corresponding testing set exhibiting a pronounced fluorescent background in the Raman spectra, the *DoH* is determined with an average absolute deviation of 0.0057.

1. Introduction

For safe transportation and long-term storage of green hydrogen (H_2) at reasonable energy densities, a large variety of storage technologies is available. Besides by liquefaction or compression [1,2], H_2 can also be stored by physical adsorption [3,4], by metal hydrides [5,6] or by fluid hydrides such as ammonia [7,8] and methanol [9,10]. A further option is the utilization of liquid organic hydrogen carriers (LOHCs) which are considered to be an important technology in the thrive of the transition towards a carbon-emission-free energy system [11–17]. LOHC systems have the ability to reversibly bind or release H_2 in a chemical hydrogenation or dehydrogenation reaction. For LOHC systems based on aromatic/alicyclic hydrocarbons, numerous investigations have recently been performed for determining their thermophysical properties. Examples are the technically relevant LOHC systems based on benzyltoluene (H0-BT) [18,19] and dibenzyltoluene (H0-DBT) [20,21]. In this context, diphenylmethane (H0-DPM) has been studied as a reference LOHC system [22–26] due to the absence of the methyl group which hampers systematic investigations due to the resulting variety of regio- and stereoisomers. Until now, variations of the degree of hydrogenation (*DoH*), which is defined as the ratio of the amount of reversibly bonded H_2 to the maximum H_2 uptake capacity of the LOHC system, could evidence a strong dependency of the thermophysical properties on the *DoH* [26,27]. For example, differences in the interfacial tension and the dynamic viscosity between the hydrogenated and dehydrogenated LOHC derivates of up to about (20 and 70)% [26] and (20 and 55)% [19] have been reported for the DPM- and BT-based systems. Therefore, knowledge of the *DoH* of a given LOHC system is not only needed for an efficient process design, but is also important to optimize the hydrogenation and dehydrogenation reaction equipment. Typically, the *DoH* can be determined by densimetry [20], rotational viscometry [20], gas chromatography (GC) [28], or nuclear magnetic resonance (NMR) [29,30].

* Corresponding author.
E-mail addresses: julius.jander@fau.de (J.H. Jander), michael.rausch@fau.de (M.H. Rausch), peter.wasserscheid@fau.de (P. Wasserscheid), andreas.p.froeba@fau.de (A.P. Fröba).

https://doi.org/10.1016/j.ijhydene.2024.06.357
Received 28 March 2024; Received in revised form 21 May 2024; Accepted 26 June 2024
Available online 4 July 2024

Abbreviations

AAD	Average absolute deviation
AARD	Average absolute relative deviation
BT, H0-BT	Benzyltoluene
DBT, H0-DBT	Dibenzyltoluene
H12-DPM	Dicyclohexylmethane
DM	Dichroic mirror
DPM, H0-DPM	Diphenylmethane
H6-DPM	Cyclohexylphenylmethane
DoH	Degree of hydrogenation
F, H0–F	Fluorene
GC	Gas chromatography
GC-FID	Gas chromatography with coupled flame ionization detection
H12–F	Perhydrofluorene
H	Horizontal
LOHC	Liquid organic hydrogen carrier
NMR	Nuclear magnet resonance
V	Vertical

One further method for the determination of the *DoH* is Raman spectroscopy which has been studied at ambient temperature in Refs. [20,31] for the DBT-based LOHC system. Recently, the application of depolarized Raman spectroscopy for the determination of the *DoH* for the DPM-based LOHC system at temperatures up to 573 K has been demonstrated [32]. Here, Raman bands characteristic for the hydrogen-lean and hydrogen-rich components could be identified and were analyzed in binary mixtures of the unloaded diphenylmethane (H0-DPM) and its fully hydrogenated counterpart dicyclohexylmethane (H12-DPM). From these investigations, a temperature-independent calibration could be obtained. This allowed for the determination of the *DoH* in technical mixtures from deliberately stopped hydrogenation reactions comprising also the intermediate product cyclohexylphenylmethane (H6-DPM) over the entire temperature range up to 573 K with average absolute deviations of 0.018 from *DoH* values determined by GC. On a laboratory scale, the application of Raman spectroscopy for the determination of the *DoH* results in larger uncertainties compared to GC, NMR, or densimetry. In technical applications, however, Raman spectroscopy outperforms these methods due to its inline applicability, e.g., during reaction processes. It should therefore enable real-time monitoring without the need for sampling. In addition, Raman sensors can be designed with small space requirements and allow for a fully automatized determination of the *DoH*.

In the first part of this work, our previous investigations are extended for the DPM-based LOHC system with respect to the analysis of technical influences present in hydrogenation or dehydrogenation reactions in form of convection as well as reaction by-products, i.e. fluorene (F, H0-F) and perhydrofluorene (H12-F). In the second part, the transferability of the calibration developed for the DPM-based system to the similar BT-based LOHC system is addressed. Finally, a novel approach for the determination of the *DoH* of the latter LOHC system at temperatures between (303 and 473) K is presented, which is based on the analysis of the unpolarized Raman signal without the need for polarization optics or filters.

2. Experimental section

2.1. Materials and sample preparation

The pure substances used in this work are itemized in Table 1 together with their CAS registry number, source, *DoH*, the purity given either as the ratio of peak areas in the chromatogram from gas chromatography with coupled flame ionization detection (GC-FID), in mass or mole fraction w and y, and with the applied purification steps.

Table 1
– Pure substances used in this work.

Substance	CAS registry number	Source	*DoH*[a]	Purity	Purification method
H0-DPM	101-81-5	Sigma Aldrich	0.000	$w = 0.998$[b]	degassed
H12-DPM	3178-23-2	self-made	0.999	0.990[c] 0.992[d]	degassed
H0-fluorene (H0-F)	86-73-7	Sigma Aldrich	0.000	$w = 0.985$[b]	none
H12-fluorene (H12-F)	5744-03-6	self-made	0.994	0.984[c] 0.996[d]	filtered and degassed
H0-o-BT	713-36-0	self-made	0.007	0.980[c] 0.995[d]	degassed
H0-p-BT	620-83-7	self-made	0.002	0.979[c] 0.998[d]	degassed
H12-o-BT	*cis*: 54824-04-3 *trans*: 54823-94-8	self-made	0.997	0.985[c] 0.991[d]	degassed
H12-p-BT	*cis*: 54823-97-1 *trans*: 54823-98-2	self-made	1.000	0.979[c] 0.989[d]	degassed
H0-iso-BT ($x_{H0\text{-}o\text{-}BT} = 0.4676$, $x_{H0\text{-}m\text{-}BT} = 0.0539$, $x_{H0\text{-}p\text{-}BT} = 0.4785$)[e]	27776-01-8	Eastman (Marlotherm LH)	0.000	0.993[c] 0.994[d]	degassed
H12-iso-BT ($x_{H12\text{-}o\text{-}BT} = 0.4787$, $x_{H12\text{-}m\text{-}BT} = 0.0628$, $x_{H12\text{-}p\text{-}BT} = 0.4585$)[e]	[f]	self-made	1.000	0.991[c,d]	filtered and degassed
Hydrogen	1333-74-0	Linde plc		$y = 0.999999$[b]	none
Argon	7440-37-1	Air Liquide S.A.		$y = 0.99999$[b]	none

[a] From GC-FID analysis considering individual peak areas of the H0-, H6-, or H12-compounds.
[b] Purity stated in the supplier's certificate.
[c] Purity determined by GC-FID.
[d] Purity determined by GC-FID considering the ratio of all LOHC-specific peak areas to all other contributions including impurities.
[e] Ratio of peak areas in the GC-FID chromatograms taking into consideration only species of the isomeric mixture.
[f] The CAS numbers of H12-o- and H12-p-BT are given in the Table. For *cis*-H12-m-BT and *trans*-H12-m-BT the CAS number is 54823-97-1 and 54823-98-2.

The *DoH* of the pure samples was analyzed by GC-FID where for the evaluation of the peak areas of the spectra, impurities were neglected. Nevertheless, the latter are considered in the specification of the sample purity. H12-DPM is identical with "batch C" in Refs. [23,26,32] and was obtained by catalytic hydrogenation [33] from commercial H0-DPM (Sigma Aldrich). H12-F corresponds to the same batch described in Ref. [34] where also details on the synthesis and the analysis using GC-FID can be found. The commercially available BT (Marlotherm LH, Eastman) comprises all three regioisomers of BT. The corresponding sample H0-iso-BT directly used in the present study stems from a different batch of Marlotherm LH than that which was hydrogenated by catalytic hydrogenation as described in the Supporting Information in Ref. [19] to obtain the used H12-iso- BT sample. Therefore, the regioisomeric compositions of the studied samples H0-iso-BT and H12-iso-BT differ slightly. The synthesis of pure H0-ortho (o)-BT, H0-para (p)-BT as well as the hydrogenated counterparts H12-o-BT and H12-p-BT from the corresponding regioisomers of methylbenzophenone by hydrodeoxygenation is detailed in Ref. [19].

With the exception of the technical mixture from a deliberately stopped hydrogenation reaction of H0-iso-BT (BT-R50), the mixtures listed in Table 2 were prepared on a balance with a precision of 0.1 mg and an estimated expanded uncertainty ($k = 2$) of 1 mg using the pure chemicals listed in Table 1. For the mixtures DPM-F3, DPM-F10, and DPM-F20, the numbers in their sample names indicate the mole fraction of fluorene at a constant *DoH* of about 0.50 in percent. For all other mixtures, the last number in the sample name corresponds to the targeted *DoH* in percent. The mixtures o-BT25, o-BT50, and o-BT75 were created by mixing H0-o-BT and H12-o-BT.

Impurities in the pure substances were neglected during weighing, but are considered in the final calculation of the *DoH*. As the amount of all derivates of the LOHC system was known from the GC-FID analysis, residual traces of the H0-, H6-, or H12-BT species in the pure H0- or H12-BT systems could be considered in the calculation of the *DoH* and the final composition of the mixtures. Thus, the actual *DoH* sometimes differs slightly from the targeted value. During storage and investigation of the samples, argon (Ar) was used as inert atmosphere.

2.2. Raman setup

The optical setup employed for the acquisition of the Raman spectra within this work has already been described in detail in Refs. [35,36]. In the following, only the main features of the setup will be reviewed. For the excitation of the scattered light, a diode-pumped solid-state laser (Cobolt Samba, Hübner Photonics, $\lambda_0 = 532.2$ nm) operated at an output power of 500 mW was used. The laser beam was guided to the sample cells by lenses and mirrors, where a dichroic mirror (DM) was placed in front of the sample cells to allow for the acquisition of Raman spectra in 180° backscattering configuration. In front of the DM, the combination of a lambda half ($\lambda/2$)-waveplate and a polarization beam splitter (PBS) allows for the attenuation of the laser beam passing through the sample cells. Here, the PBS was adjusted to transmit vertically (V) polarized light only.

A further $\lambda/2$-waveplate placed between the PBS and the DM enabled the alternation of the polarization of the incident laser beam between V and horizontal (H). The Raman-scattered light was collected by a lens array and focused on a fiber connected to a spectrometer (QEPro, Ocean Optics). In front of the fiber opening, a razor-edge long-pass filter was mounted. In addition, a broadband PBS located in the lens array ensures that only V-polarized Raman-scattered light enters the fiber. Thus, both polarized and depolarized Raman spectra (I_{VV} and I_{HV}) could be obtained alternately after rotation of the corresponding $\lambda/2$-waveplate in steps of 45°.

2.3. Investigations in the stainless-steel cell

For the investigation of the influence of forced convection caused by

Table 2
– Sample mixtures investigated in this work.

Sample	*DoH*[a]	Composition[b]	Purity[c]
DPM-B50	0.498	$x_{H0\text{-}DPM} = 0.502$ $x_{H12\text{-}DPM} = 0.498$	$w = 0.995$
Samples comprising fluorene derivates			
DPM-F3 ($x_{F,effective} = 0.030$)	0.498	$x_{H0\text{-}DPM} = 0.487$ $x_{H12\text{-}DPM} = 0.483$ $x_{H0\text{-}F} = 0.015$ $x_{H6\text{-}F} = 0.000$ $x_{H12\text{-}F} = 0.015$	$w = 0.995$
DPM-F10 ($x_{F,effective} = 0.100$)	0.498	$x_{H0\text{-}DPM} = 0.452$ $x_{H12\text{-}DPM} = 0.448$ $x_{H0\text{-}F} = 0.050$ $x_{H6\text{-}F} = 0.001$ $x_{H12\text{-}F} = 0.049$	$w = 0.994$
DPM-F20 ($x_{F,effective} = 0.200$)	0.495	$x_{H0\text{-}DPM} = 0.404$ $x_{H12\text{-}DPM} = 0.396$ $x_{H0\text{-}F} = 0.100$ $x_{H6\text{-}F} = 0.001$ $x_{H12\text{-}F} = 0.099$	$w = 0.994$
Samples comprising BT derivates			
iso-BT10	0.099	$x_{H0\text{-}iso\text{-}BT} = 0.901$ $x_{H6\text{-}iso\text{-}BT} = 0.001$ $x_{H12\text{-}iso\text{-}BT} = 0.098$	$w = 0.994$
iso-BT30	0.296	$x_{H0\text{-}iso\text{-}BT} = 0.703$ $x_{H6\text{-}iso\text{-}BT} = 0.001$ $x_{H12\text{-}iso\text{-}BT} = 0.296$	$w = 0.993$
iso-BT50	0.496	$x_{H0\text{-}iso\text{-}BT} = 0.504$ $x_{H6\text{-}iso\text{-}BT} = 0.000$ $x_{H12\text{-}iso\text{-}BT} = 0.496$	$w = 0.992$
iso-BT70	0.696	$x_{H0\text{-}iso\text{-}BT} = 0.304$ $x_{H6\text{-}iso\text{-}BT} = 0.000$ $x_{H12\text{-}iso\text{-}BT} = 0.696$	$w = 0.992$
iso-BT90	0.898	$x_{H0\text{-}iso\text{-}BT} = 0.102$ $x_{H6\text{-}iso\text{-}BT} = 0.000$ $x_{H12\text{-}iso\text{-}BT} = 0.898$	$w = 0.991$
BT-R50	0.514	$x_{H0\text{-}o\text{-}BT} = 0.198$ $x_{H0\text{-}m\text{-}BT} = 0.025$ $x_{H0\text{-}p\text{-}BT} = 0.190$ $x_{H6\text{-}BT} = 0.146$ $x_{H12\text{-}o\text{-}BT} = 0.201$ $x_{H12\text{-}m\text{-}BT} = 0.028$ $x_{H12\text{-}p\text{-}BT} = 0.212$	$w = 0.999$
o-BT25	0.254	$x_{H0\text{-}o\text{-}BT} = 0.741$ $x_{H6\text{-}o\text{-}BT} = 0.010$ $x_{H12\text{-}o\text{-}BT} = 0.249$	$w = 0.994$
o-BT50	0.497	$x_{H0\text{-}o\text{-}BT} = 0.499$ $x_{H6\text{-}o\text{-}BT} = 0.007$ $x_{H12\text{-}o\text{-}BT} = 0.494$	$w = 0.993$
o-BT75	0.749	$x_{H0\text{-}o\text{-}BT} = 0.249$ $x_{H6\text{-}o\text{-}BT} = 0.003$ $x_{H12\text{-}o\text{-}BT} = 0.748$	$w = 0.992$
(H0-o/H12-p)-BT33	0.330	$x_{H0\text{-}o\text{-}BT} = 0.665$ $x_{H6\text{-}o\text{-}BT} = 0.009$ $x_{H12\text{-}o\text{-}BT} = 0.000$ $x_{H0\text{-}p\text{-}BT} = 0.001$ $x_{H6\text{-}p\text{-}BT} = 0.000$ $x_{H12\text{-}p\text{-}BT} = 0.325$	$w = 0.993$
(H0-o/H12-p)-BT67	0.668	$x_{H0\text{-}o\text{-}BT} = 0.329$ $x_{H6\text{-}o\text{-}BT} = 0.004$ $x_{H12\text{-}o\text{-}BT} = 0.000$ $x_{H0\text{-}p\text{-}BT} = 0.002$ $x_{H6\text{-}p\text{-}BT} = 0.000$ $x_{H12\text{-}p\text{-}BT} = 0.665$	$w = 0.991$
(H0-p/H12-o)-BT33	0.325	$x_{H0\text{-}o\text{-}BT} = 0.001$ $x_{H6\text{-}o\text{-}BT} = 0.000$ $x_{H12\text{-}o\text{-}BT} = 0.326$ $x_{H0\text{-}p\text{-}BT} = 0.671$ $x_{H6\text{-}p\text{-}BT} = 0.002$ $x_{H12\text{-}p\text{-}BT} = 0.000$	$w = 0.996$
(H0-p/H12-o)-BT67	0.665	$x_{H0\text{-}o\text{-}BT} = 0.002$ $x_{H6\text{-}o\text{-}BT} = 0.000$ $x_{H12\text{-}o\text{-}BT} = 0.666$ $x_{H0\text{-}p\text{-}BT} = 0.331$ $x_{H6\text{-}p\text{-}BT} = 0.001$ $x_{H12\text{-}p\text{-}BT} = 0.000$	$w = 0.993$

[a] Calculated based on the amounts of the H0-, H6-, or H12-species in the pure substances under consideration of their purity.
[b] Calculated from the results of GC-FID neglecting all further contributions in the sample.
[c] Obtained by consideration of the purity of the initial substances used for mixing.

stirring or a H_2 gas flow on the quality of Raman measurements for DPM-B50, the same sample cell as detailed in Ref. [23] was used. For this, a H_2 reservoir was connected to the inlet at the bottom of the cell. By using a valve, the gas flow into the liquid phase was controlled. The T control was realized *via* resistance heating in combination with a T measurement by using a Pt100Ω resistance probe located close to the outer cell wall. The reported T is the average of two further Pt100Ω resistance probes placed in the cell wall in the vicinity of the gas and liquid phase close to the center of the cell.

After filling about 80 ml of DPM-B50 at about 293 K, vacuum was applied. Thereafter, the sample was saturated with H_2 close to ambient pressure. The sample cell was then heated to the desired T of 473 K. In total 3 different measurement series were performed, where the first one was conducted without any forced convection serving as a reference in the following. For the second and the third measurement series, the sample was studied under the influence of forced convection caused by stirring or by a constant bubble flow of H_2 through the liquid phase. In the first two measurement series, 8 I_{HV} spectra were obtained for which the $\lambda/2$-waveplate was rotated stepwise by 90° over two full revolutions. Here, each I_{HV} spectrum represents an average of 6 individual spectra subsequently recorded by the spectrometer with an integration time of 5 s. For the H_2 injection in the third series, 16 subsequent individual I_{HV} spectra were obtained with an integration time of 1 s without rotation of the $\lambda/2$ waveplate.

In general, for the investigation in the stainless-steel cell, the T were measured with an estimated expanded ($k = 2$) uncertainty of $U(T) = 40$ mK considering the calibrated expanded uncertainty of the Pt100Ω resistance probes of 20 mK. For the measurements in the presence of convection, $U(T)$ is estimated to be 0.1 K.

2.4. Investigations in fused silica cuvettes

All DPM-based systems containing H0- and H12-F as well as the BT-based samples have been studied in glass cuvettes made of fused silica (111-10-40, Helma Analytics) placed inside a cuvette holder which was controlled by resistance heating. Here, T was measured by a Pt100Ω resistance probe with an uncertainty of $U(T) = 20$ mK ($k = 2$). The cuvette holder was kept at the same T while all samples of interest were studied consecutively. For each state point, about 5–6 ml of sample was filled into the cuvette by a glass pipet. Argon was filled above the liquid sample in the cuvette to minimize contact with air. A further Pt100Ω resistance probe with $U(T) = 20$ mK ($k = 2$) was immersed in the liquid from the top of the cuvette through a small borehole in a plug made of PTFE. In this way, the cuvette was sealed against the surrounding atmosphere. For investigations at elevated T, the prepared cuvette was gradually pre-heated using a heat gun to prevent damage to the cuvette from thermal shock when it is inserted into the cuvette holder. For most systems, the laser power irradiating the cuvette was 100 mW. At $T \approx$ 473 K, however, absorption of the laser light was indicated by a thermal lens effect leading to a broadening of the laser beam for the mixtures comprising fluorene and the pure BT isomers. This could be overcome by the reduction of the laser power to 20 mW.

For all samples studied in cuvettes, 8 I_{VV} and 8 I_{HV} spectra were recorded. By the stepwise revolution of the $\lambda/2$-waveplate in front of the DM in increments of 45°, the spectra were recorded alternately one after another. The final spectra represent the averages of (3 or 5) individual spectra with integration times between (10 or 6) s. The reported T is the average of the T measured by the probe inside the liquid during the acquisition period of the 16 spectra. Overall, a stability better than 1.8 mK at $T \approx 303$ K and better than 3.4 mK at larger T could be achieved.

3. Data evaluation

3.1. Evaluation of the depolarized spectra

With the exception of the sample DPM-B50 disturbed by H_2 bubbles, where 16 I_{HV} spectra were acquired, 8 I_{HV} spectra were analyzed using the procedure described in detail in Ref. [32]. In the following, a brief summary of the evaluation principle is provided and the minor changes performed in the peak-fitting routine within this work are described.

The decisive reason for choosing an evaluation of the depolarized Raman spectra of the DPM-based systems investigated in Ref. [32] was the unambiguous assignment of Raman signatures to the hydrogenated and dehydrogenated carbon rings such that their intensity ratio gave access to the *DoH*. Despite the significantly lower signal intensity in the depolarized I_{HV} spectra in comparison with the polarized I_{VV} spectra, it was only possible in the former to identify a frequency range where the Raman signature of the CH_2 symmetrical-stretching vibration associated with the hydrogenated rings of H12-DPM vanishes in the limiting case of pure H0-DPM. In the polarized I_{VV} spectrum, however, also the symmetric CH_2 vibration associated with the methylene group between the two aromatic rings of H0-DPM [32,37] is present in that specific frequency range.

For the evaluation of the depolarized spectra, the individual I_{HV} spectra were normalized by the standard-normal-variate transformation [38] and averaged. The background contribution was then removed by a baseline-subtraction routine [39]. Thereafter, the resulting spectrum was fitted by the sum of 6 Gaussian peaks in the range between (2800 and 3150) cm^{-1} by utilizing the fmincon function from the Optimization Toolbox implemented in MATLAB [40]. For this, the root-sum-squared deviation (RSSD) between the recorded spectrum and the sum of the Gaussian peaks was defined as the objective function and minimized by adjusting the central peak positions, the widths, and the heights of the peaks. To improve the robustness of the fit, the following constraints were applied: The central positions of the peaks were limited only to the considered frequency range, the full-width-at-half-maximum was set in the range between (10 and 60) cm^{-1}, and a minimum peak height of 1% of the maximum intensity within the analyzed frequency range was postulated.

From optimized peak parameters which describe the experimental spectrum best, the area of the of the Gaussian peaks with center positions smaller than 2870 cm^{-1} as well as larger than 3000 cm^{-1} were assigned with the intensities I_{H12} and I_{H0} [32] from which the intensity ratio

$$I_r = \frac{I_{H0}}{I_{H12}} \tag{1}$$

was evaluated. From I_r, the *DoH* can be calculated *via*

$$DoH = \frac{1}{1 + K_{DPM,all} \cdot I_r} \tag{2}$$

using the T-independent calibration factor $K_{DPM,all} = 0.65818$ determined in Ref. [32]. The expanded uncertainty $U(I_r)$ was estimated from the residual RSSD of the peak-fit routine under consideration of the error resulting from the baseline subtraction. The error induced from the baseline correction was calculated from the deviation between the fitted baseline obtained from the background removal procedure and a combination of two linear baselines interconnecting the first and last datapoint of the frequencies considered in the peak fit routine which intersect on the fitted baseline at the point of its largest curvature. $U(DoH)$ can be calculated by error propagation in quadrature from $U(I_r)$ together with $U(K_{DPM,all}) = 0.051$ [32].

3.2. Evaluation of the unpolarized Raman spectra

For the initial evaluation process of the depolarized spectra, systematic deviations of the *DoH* determined by Raman spectroscopy according to Eq. (2) with $K_{DPM,all} = 0.65818$ from the values known from the analysis *via* GC-FID as well as from defined mixtures (DoH_{ref}) given in Table 1 and Table 2 became apparent for the BT-based samples. For all T, absolute deviations of about +0.1 were found for H0-iso-BT and decreased linearly towards ≈ 0 for H12-iso-BT. Here, contributions from the additional methyl group of the BT-based LOHC system superimpose with the symmetric CH_2 vibration of the hydrogenated rings at ≈ 2840 cm^{-1}. For the analogous case of toluene-d_5, the origin of these bands is referred to the Fermi resonance of the first overtone of the asymmetric CH_3 bending along with the fundamental symmetric CH_3 stretching [41].

Therefore, a novel approach for the evaluation of the Raman spectra for the BT-based system was adopted, which is based on indirect hard modeling (IHM) proposed in Refs. [42–45]. Since no direct advantage is given by a polarization-dependent analysis of spectra in terms of band separation, the unpolarized spectra, i.e. I_0=$I_{HV} + I_{VV}$, have been focused on. This allows the evaluation of the *DoH* on setups or in process equipment, e.g., in hydrogenation reactors, by commercial Raman sensors operating in backscattering configuration without the need of complex polarization optics or filters.

For H0- and H12-iso-BT, I_0 was calculated from the sum of the averages of 8 I_{VV} and 8 I_{HV} spectra. Thereafter, the background was removed by a baseline-removal routine [46]. For this, regions in the I_0 spectra were identified where no Raman signatures are expected. The background-corrected spectra of H0- and H12-iso-BT were fitted in the full frequency range between ν = (2500 and 3250) cm^{-1} by the sum of 13 and 10 pseudo-Voigt profiles, which represent an approximations of Voigt profiles using linear combinations of Gaussian and Lorentzian curves instead of their convolution. The approximation of the convolution employed in this work is given by

$$V(\nu,\alpha,\beta,\Gamma,\nu_0) = \beta\alpha \exp\left[-\frac{4\ln 2(\nu-\nu_0)^2}{\Gamma^2}\right] + (1-\beta)\alpha\frac{\Gamma^2}{(\nu-\nu_0)^2+\Gamma^2}, \quad (3)$$

where the parameters α, Γ, ν_0, and β correspond to the height, width, central position, and the Gauss-Lorentzian ratio, respectively [47,48]. To provide a temperature-independent methodology, only the spectra obtained for H0- and H12-iso-BT at the median T of the investigations, *i.e.*, $T \approx 373$ K, are considered in the subsequent evaluation procedure. The corresponding parameters α, Γ, ν_0, and β of the 13 or 10 individual pseudo-Voigt profiles described by Eq. (3) are summarized in Table S1 of the Supporting Information.

Focusing on the frequency range between ν = (2800 and 3100) cm^{-1}, the raw I_0 spectra of the mixtures were modelled utilizing the spectral information of H0- and H12-iso-BT at $T \approx 373$ K together with a second-order polynomial to account for the background contribution. For this, the RSSD between the measured I_0 spectra and the modelled ones was minimized using the fmincon algorithm from the Optimization Toolbox integrated in MATLAB [40] by adjusting the contributions from the pure H0- and H12-iso-BT models as well as the polynomial. Furthermore, the central peak positions ν_0 of the underlying pseudo-Voigt profiles were allowed to be adjusted independently within 1% to account for any spectral shifts in the mixtures. With the results of the modelling procedure, the individual intensity areas of H0- and H12-iso-BT in the I_0 spectra of the mixtures were calculated to obtain I_r *via* Eq. (1).

To determine the calibration factor K_{BT}, I_r and the known DoH_{ref} in Table 2 were correlated by Eq. (2) for the binary mixtures of H0- and H12-iso-BT at the individual T. Similarly, $K_{BT,all}$ was determined by considering all data for these systems at all T investigated. The expanded (k = 2) uncertainty $U(I_r)$ was estimated by error propagation in quadrature, where the expanded (k = 2) uncertainties in I_{H0} and I_{H12} were determined with help of the RSSD between the measured and the modelled spectra, considering also the influence of the background. $U(K)$ was received from the quality of the fit according to Eq. (2), where the correlated data were weighted by the inverse of their relative uncertainty.

4. Results and discussion

In the following, first the results of the influence of convection and reaction byproducts on the determination of the *DoH* for the DPM-based LOHC system are presented, where the recorded depolarized I_{HV} Raman spectra are evaluated using the procedure and calibration according to Ref. [32] described in Section 3.1. Thereafter, the results for the new calibration of the BT-based LOHC system are given, for which a novel methodology comprising indirect hard modeling (IHM) of the unpolarized (I_0=$I_{VV} + I_{HV}$) Raman spectra has been chosen.

4.1. Determination of the DoH for DPM-based LOHC systems using depolarized I_{HV} Raman spectra

For the sample DPM-B50, the results for the *DoH* calculated by Eq. (2) using I_r obtained from the evaluation of the depolarized I_{HV} spectra are summarized in the first three rows of Table 3. There, also the results for the DPM-based samples containing H0- and H12-F are given.

For the sample DPM-B50 without any disturbance, the *DoH* of could be determined using K_{all} from Ref. [32] with an absolute deviation of about +0.018 with respect to DoH_{ref}, which is within the uncertainty of $U(DoH)$ = 0.019. This further proves the transferability of K_{all} to different setups. Forced convection by stirring the liquid sample results in DoH = 0.525. This value differs from DoH_{ref}, but it is shifted by only +0.009 with respect to *DoH* determined in the measurement without convection. The result of *DoH* obtained from Raman spectroscopy while forced convection is caused by a H_2-gas stream reproduces the *DoH* obtained for the measurement without convection. In this case, only a slight increase of $U(DoH)$ could be observed. Comparing the obtained *DoH* values on the same setup for the same mixture and considering the measurement uncertainty, the conclusion can be drawn that forced convection influences the determination of *DoH* only slightly within uncertainties.

For the determination of the *DoH* for the DPM-based samples comprising H0- and H12-F at mole fractions of about 0.03, 0.10, and 0.20, the results are shown in Fig. 1.

At $T \approx 303$ K, the results of the *DoH* in comparison to DoH_{ref} are almost unaffected by the presence of H0-/H12-F. Here, mole fractions of 0.03 and 0.10 of H0-/H12-F lead to a slight *DoH* deviation of −0.008

Table 3
– Results for the *DoH* calculated by Eq. (2) using $K_{DPM,all}$ from Ref. [32] and the absolute deviation from DoH_{ref} given in Table 2.[a]

Sample	T/K	I_r	$U(I_r)$	*DoH*	U(*DoH*)	*DoH* – DoH_{ref}
DPM-B50	473.73	1.426	0.013	0.516	0.019	0.018
DPM-B50 + stirring	473.8[b]	1.373	0.011	0.525	0.019	0.027
DPM-B50 + H_2 flow	473.8[b]	1.424	0.015	0.516	0.020	0.018
DPM-F3	303.02	1.567	0.062	0.492	0.022	−0.006
DPM-F10	303.18	1.57	0.25	0.492	0.044	−0.006
DPM-F20	303.11	1.63	0.61	0.482	0.095	−0.013
DPM-F3	473.14	1.80	0.12	0.458	0.025	−0.040
DPM-F10	473.13	1.49	0.43	0.505	0.075	0.007
DPM-F20	473.14	2.2	1.8	0.41	0.20	−0.085

[a] $U(T)$ = 0.02 K if not stated otherwise, $U(I_r)$ and $U(DoH)$ are given in the table. All uncertainties are given on a confidence level of 0.95.
[b] $U(T)$ = 0.1 K.

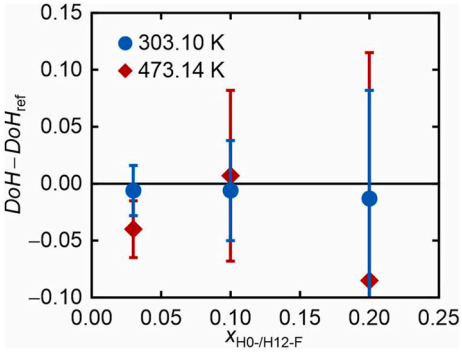

Fig. 1. Absolute deviation of *DoH* calculated by Eq. (2) using the depolarized I_{HV} spectra of the quaternary system H0-/H12-DPM with H0-/H12-F from the DoH_{ref} of about 0.50 as a function of H0-/H12-F mole fraction. (For interpretation of the references to color in this figure legend, the reader is referred to the Web version of this article.)

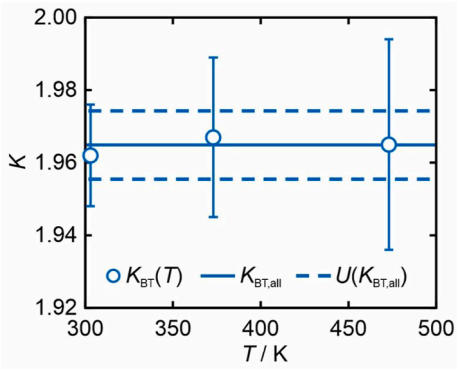

Fig. 2. Calibration factors K_{BT} and $K_{BT,all}$ obtained from the correlation of I_r and DoH_{ref} according to Eq. (2) for the BT-based LOHC system. (For interpretation of the references to color in this figure legend, the reader is referred to the Web version of this article.)

which increases to −0.014 at a mole fraction of 0.20. At $T \approx 473$ K, the influence of the fluorene derivates becomes more dominant, where the most pronounced deviation of −0.086 from the known DoH_{ref} is present for the largest mole fraction. With increasing fluorene-derivate content, there is a considerable increase of *U*(*DoH*) which nearly doubles from (303 to 473) K. This behavior mainly arises from the strong fluorescent background which increases with increasing fluorene-derivate content and *T*. Here, the relatively weak signal intensity of the depolarized spectra I_{HV} is almost indistinguishable from the background and noise. Nevertheless, it should be noted that already a H0-/H12-F mole fraction of 0.03 would correspond to a LOHC batch processed under very harsh dehydrogenation conditions with deep H_2 unloading over multiple cycles. For comparable LOHC systems based on BT and DBT, corresponding fluorene-based species were found with GC area ratios of less than 0.02 and 0.04 after several dehydrogenation reactions lasting up to 80 h at $T = 563$ K and at a H_2 partial pressure of 0.1 MPa [49].

4.2. Determination of the DoH for BT-based LOHC systems using unpolarized I_0 Raman spectra

The calibration factors for the BT-based LOHC system K_{BT} obtained with help of the samples iso-BT10 to iso-BT90 according to Eq. (2) are summarized in Table 4. Fig. 2 shows these constants for the different *T* investigated as well as for the case that all I_r data are considered for the correlation, resulting in the *T*-independent calibration constant $K_{BT,all}$ which is displayed as a horizontal line. To illustrate the behavior of the correlation used for calibration, Eq. (2), the employed DoH_{ref} data are also shown as a function of I_r for the binary mixtures of H0-/H12-iso-BT and for the technical mixture BT-R50 in Fig. 3. Here, the resulting

Table 4
– Calibration factors K_{BT} and $K_{BT,all}$ obtained from the correlation of I_r as a function of DoH_{ref} for the BT-based LOHC system. The I_r and DoH_{ref} values correlated according to Eq. (2) correspond to binary mixtures of iso-BT10 to iso-BT90 and are listed in Table 2.

T/K[a]	K_{BT}	$U(K_{BT})$[b]
303.08 ± 0.05	1.945	0.013
373.19 ± 0.04	1.943	0.020
473.00 ± 0.18	1.922	0.015
	$K_{BT,all}$	$U(K_{BT,all})$[b]
303–473	1.9365	0.0089

[a] The reported value corresponds to the average of the *T* specified in Table 5 for the samples iso-BT10 to iso-BT90. *U*(*T*) is the maximum deviation of the individual *T* from the average value and given behind the latter.

[b] Uncertainty ($k = 2$) of K_{BT} and $K_{BT,all}$ obtained from the quality of the fit considering the measurement data for I_r weighted by the inverse of their relative uncertainties.

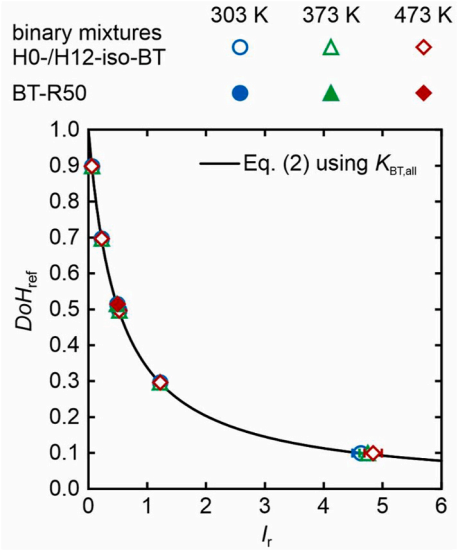

Fig. 3. DoH_{ref} as a function of I_r obtained by Eq. (1) applying the IHM procedure for the binary BT-based sample mixtures iso-BT10 to iso-BT90 and H12-iso-BT (open symbols) as well as the technical mixture BT-R50 (closed symbols) at *T* between (303 and 473) K. The drawn line represents Eq. (2) using $K_{BT,all}$. (For interpretation of the references to color in this figure legend, the reader is referred to the Web version of this article.)

correlation using $K_{BT,all}$ is included as well. The I_r data of all BT-based mixtures are summarized in Table 5 together with the *DoH* calculated according to Eq. (2) using $K_{BT,all}$.

Fig. 2 shows that the K_{BT} values obtained at the individual *T* over the full *T* range between (303 and 473) K and $K_{BT,all}$ agree within uncertainty, which suggests a *T*-independent treatment of the calibration using $K_{BT,all}$. These findings are in agreement with our investigations for the DPM-based system, where the calibration values were found to be independent of *T* between (303 and 573) K [32]. Further studies from our group and in the literature report also a *T*-independent calibration factor, e.g., for the liquid-liquid system *n*-octacosane and water [50], the liquid-gas systems of methanol with H_2 [36], 1-hexanol or *n*-hexane with sulfur hexafluoride or R143a [35], 1-hexanol with CO_2 [51], and acetone or dimethyl sulfoxide with CO_2 [52]. The *T*-independent nature of the calibration constant is further indicated in Fig. 3, where the individual I_r at different *T* of the binary mixtures match at given DoH_{ref} within $U(I_r)$ and, therefore, are well-described by Eq. (2) using $K_{BT,all}$. The same statement holds for the technical mixture BT-R50, which comprises a mole fraction of about 0.146 of the partially hydrogenated

Table 5
– *DoH* of the BT-based samples determined by Raman spectroscopy *via* Eq. (2) using $K_{BT,all}$ given in Tables 4 and I_r obtained according to Eq. (1). The absolute deviation of *DoH* refers to the reference value DoH_{ref} which is specified in Table 1 and Table 2.[a]

Sample	*T*/K	I_r	$U(I_r)$	*DoH*	*U* (*DoH*)	*DoH* – DoH_{ref}
calibration set						
***T* = 303 K**						
iso-BT10	303.13	4.63	0.14	0.0990	0.0027	0.0000
iso-BT30	303.11	1.215	0.016	0.2952	0.0029	−0.0008
iso-BT50	303.09	0.5189	0.0073	0.4952	0.0037	−0.0008
iso-BT70	303.00	0.2219	0.0051	0.6964	0.0050	0.0004
iso-BT90	303.08	0.0561	0.0042	0.9007	0.0067	0.0027
***T* = 373 K**						
iso-BT10	373.23	4.75	0.14	0.0968	0.0026	−0.0022
iso-BT30	373.19	1.211	0.015	0.2959	0.0028	−0.0001
iso-BT50	373.09	0.518	0.0068	0.4956	0.0035	−0.0004
iso-BT70	373.22	0.2216	0.0047	0.6967	0.0046	0.0007
iso-BT90	373.21	0.0549	0.0038	0.9026	0.0061	0.0046
***T* = 473 K**						
iso-BT10	472.62	4.84	0.15	0.0951	0.0027	−0.0039
iso-BT30	473.17	1.216	0.015	0.2950	0.0028	−0.0010
iso-BT50	473.18	0.5182	0.0068	0.4955	0.0035	−0.0005
iso-BT70	472.93	0.2216	0.0046	0.6967	0.0045	0.0007
iso-BT90	473.12	0.054	0.0037	0.9041	0.0060	0.0061
testing set						
***T* = 303 K**						
BT-R50	303.10	0.4849	0.0089	0.5121	0.0047	−0.0019
o-BT25	303.03	1.523	0.029	0.2505	0.0037	−0.0035
o-BT50	303.03	0.5125	0.0075	0.4983	0.0038	0.0013
o-BT75	303.03	0.1688	0.0043	0.7509	0.0048	0.0019
(H0-o/H12-p)-BT33	303.06	0.962	0.035	0.3460	0.0083	0.0160
(H0-o/H12-p)-BT67	302.92	0.2363	0.0076	0.6829	0.0070	0.0149
(H0-p/H12-o)-BT33	303.04	0.993	0.066	0.339	0.015	0.0140
(H0-p/H12-o)-BT67	303.00	0.232	0.015	0.687	0.014	0.0220
***T* = 373 K**						
BT-R50	373.09	0.4793	0.0082	0.5150	0.0044	0.0010
***T* = 473 K**						
BT-R50	473.19	0.4897	0.0076	0.5096	0.0041	−0.0044
o-BT25	473.12	1.50	0.13	0.253	0.016	−0.0010
o-BT50	472.86	0.515	0.024	0.497	0.012	0.0000
o-BT75	472.97	0.1753	0.0076	0.7438	0.0083	−0.0052
(H0-o/H12-p)-BT33	473.18	1.031	0.050	0.330	0.011	0.0000
(H0-o/H12-p)-BT67	473.23	0.257	0.015	0.664	0.013	−0.0040
(H0-p/H12-o)-BT33	473.17	1.037	0.036	0.3292	0.0077	0.0042
(H0-p/H12-o)-BT67	473.10	0.2585	0.0092	0.6632	0.0080	−0.0018
pure substances						
H0-iso-BT	303.04	Inf	Inf	0	–	0
	373.20	Inf	Inf	0	–	0
	473.13	600	2000	0.0008	0.0028	0.0008
H12-iso-BT	303.11	0.0000	0.0041	1.000	0.0081	0.0000
	373.10	0.0000	0.0036	1.000	0.0071	0.0000
	472.64	0.0000	0.0036	1.000	0.0071	0.0000

[a] $U(T) = 0.02$ K if not indicated otherwise. $U(I_r)$ as well as $U(DoH)$ are given in the table. All uncertainties are given on a confidence level of 0.95.

H6-iso-BT species. Therefore, $K_{BT,all}$ was used to evaluate *DoH* for all BT-based samples resulting in an average absolute deviation (AAD) of 0.0017 with a bias of +0.0004 for *DoH* – DoH_{ref} taking into account all binary calibration mixtures at all *T*.

The *DoH* evaluated according to Eq. (2) for the binary mixtures consisting of pure regioisomers of H0-BT and/or H12-BT as well as the technical mixture BT-R50 between *T* = (303 and 473) K using $K_{BT,all}$ are shown in Fig. 4. These systems represent the testing set in this study. While in the upper part of Fig. 4, a parity plot compares the obtained *DoH* with DoH_{ref}, the deviations *DoH* – DoH_{ref} are given as a function of DoH_{ref} in the lower part. In both parts of Fig. 4, deviations of ±0.02 from an ideal agreement are indicated by dashed lines.

For all systems shown in Fig. 4, the *DoH* could be determined by Raman spectroscopy with a maximum absolute deviation from DoH_{ref} of 0.022 and an AAD of 0.0057. This means that the AAD for this testing set is smaller than the corresponding average *U*(*DoH*), which is 0.0086. For the homologue series of binary mixtures based on H0-o-BT and H12-o-BT with *DoH* = (0.25, 0.50, and 0.75), the AAD is 0.0022 with an average *U*(*DoH*) of 0.0081. The samples produced from o- and p-BT isomers show slight positive deviations at *T* = 303 K. At *T* = 473 K, the measured *DoH* is closer to DoH_{ref}, resulting in total in an AAD for these mixtures of 0.010. It should be noted that the route of synthesis of the pure o- and p-BT isomers incorporated traces of highly fluorescent impurities which generally resulted in lower spectra quality and, thus, larger *U*(*DoH*) of on average 0.011 for corresponding mixtures in comparison to those of H0- and H12-iso-BT as well as the technical mixture

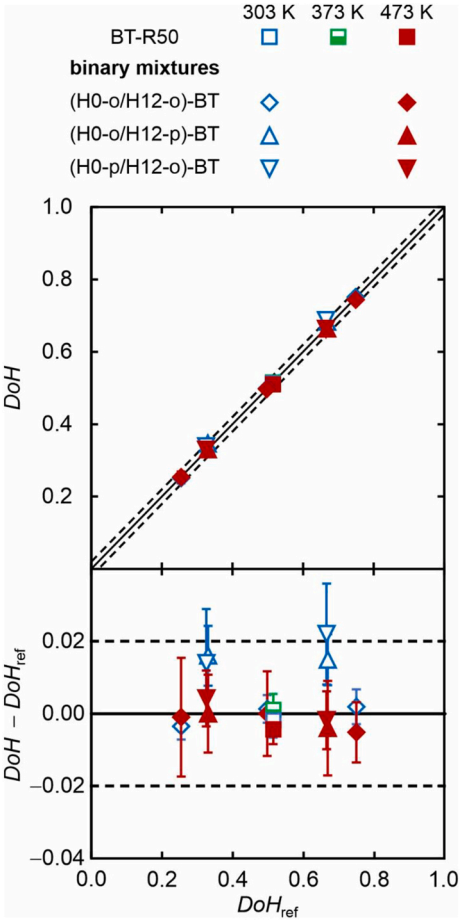

Fig. 4. Results for the *DoH* calculated according to Eq. (2) using I_r given in Table 5 and $K_{BT,all}$ from Table 4 as a function of DoH_{ref} from Table 2 for binary mixtures consisting of H0- and H12-o-BT (diamonds), H0-o- and H12-p-BT or H0-p- and H12-o-BT (triangles), as well as for the technical mixture BT-R50 (squares) at *T* ≈ 303 K (open symbols), 373 K (half-filled symbol), and 473 K (closed symbols) in form of a parity plot (upper part) and a residual plot (lower part). The dashed lines correspond to an absolute deviation of *DoH* from DoH_{ref} by ±0.02. (For interpretation of the references to color in this figure legend, the reader is referred to the Web version of this article.)

BT-R50. For BT-R50, which comprises up to nine partially hydrogenated regio- and stereoisomers of H6-BT in addition to the H0- and H12-isomers, it is remarkable that the AAD is 0.0024, the most pronounced deviation is −0.0044 at $T \approx 473$ K, and the average $U(DoH)$ is 0.0044.

In our previous publication [32], a detailed comparison with investigations using Raman spectroscopy for the determination of the *DoH* for the similar LOHC system based on DBT at ambient T [20,31] has already been performed. Therefore, only a short discussion of the literature is given in the following. Müller et al. [20] reported average relative deviations for the representation of the calibration mixtures of 2.7% and 1.2% neglecting one outlier. Furthermore, they reported an average relative deviation of 8.5% in the transfer of the calibration to five reaction mixtures with DoH_{ref} ranging from 0.39 to 0.76. In the work of Inhetveen et al. [31], the determination of *DoH* could be realized with absolute deviations smaller than 0.05 for most of the samples. In our previous work [32] focusing on the evaluation of the *DoH* for the DPM-based LOHC system using the depolarized I_{HV} spectra, the determination of the *DoH* at $T \approx 303$ K resulted in an average absolute relative deviation (AARD) obtained for the binary calibration mixtures of 2.3% or 1.0% neglecting the rather large relative deviation of the sample with a small *DoH* of about 0.1. The transfer of $K_{DPM,all}$ to the pure H6-DPM ($DoH_{ref} = 0.50$) and three reaction mixtures with DoH_{ref} of about 0.21, 0.55, and 0.81 resulted in relative deviations of (−2.9, 4.5, −0.4, and −0.8)%, respectively, where the latter was evaluated at $T \approx 423$ K. The AAD was 0.006 for all DPM-based samples studied at $T = 303$ K in Ref. [32]. This AAD is larger than that found in the present study with $K_{BT,all}$ for all mixtures of the calibration and the testing sets as well as at all T studied, where the AAD is 0.0038. To allow for a further comparison with the aforementioned references, it can be stated that the corresponding AARDs are 0.59%, 0.47%, and 1.42% for the binary calibration mixtures from iso-BT10 to iso-BT90, for the reaction mixture, and for all other mixtures, respectively, at T up to 473 K.

5. Conclusion

In the first part of this study, recent investigations on the determination of the degree of hydrogenation (*DoH*) using depolarized Raman spectroscopy [32] were extended for the diphenylmethane (DPM)-based LOHC system to process-near condition including the influence of forced convection as well as the addition of process-typical impurities in the form of fluorene (H0-F) and its hydrogenated counterpart perhydrofluorene (H12-F). Stirring of the sample and blowing H_2 bubbles through the sample at a known *DoH* of about 0.50 showed no significant influence on the results in comparison with the *DoH* determined at undisturbed conditions. The addition of H0- and H12-F at total mole fractions of 0.03, 0.10, and 0.20 at a constant *DoH* of approximately 0.50 revealed a strong reduction of the signal quality of the spectra caused by the fluorescent background at larger H0-/H12-F mole fractions, which was further deteriorated at larger T. Although the uncertainty in the determination of the *DoH* increased up to 0.20 at a H0-/H12-F mole fraction of 0.20 at $T = 473$ K, the determination of the *DoH* by Raman spectroscopy at moderate, process-relevant H0-/H12-F concentrations is still rather accurate.

In the second part of the work, calibration factors K_{BT} for the benzyltoluene (BT)-based LOHC system were determined using binary mixtures of H0- and H12-iso-BT by employing a novel evaluation method based on indirect hard modeling (IHM) of the unpolarized mixture spectra from the spectra of the two pure substances. K_{BT} was found to be independent of T within the studied range from (303 to 473) K. Therefore, the calculated T-independent calibration constant $K_{BT,all}$ resulted in an AAD of 0.0017 for the determined *DoH* from DoH_{ref} for the calibration mixtures. On this basis, the *DoH* of a testing set consisting of binary mixtures of pure ortho- and para-regioisomers of H0- and H12-BT as well as a technical mixture obtained from a deliberately stopped hydrogenation reaction of H0-iso-BT containing also numerous regio- and stereoisomers of H6-BT could be determined at T up to 473 K with an AAD of 0.0057.

In summary, this work has proven the applicability of unpolarized Raman spectroscopy in backscattering configuration for the determination of the *DoH* of the BT-based LOHC system by IHM. The findings suggest that Raman spectroscopy can be implemented for online-monitoring of the *DoH*, e.g., during reaction processes, in real time without any need for a sampling, where the results for the DPM-based system in the first part of the work indicate that effects related to process-related conditions such as moderate concentrations of reaction side products or convection seem to have no significant influence on the results.

In the future, the influence of impurities in form of methylfluorene and perhydromethylfluorene on the determination of the *DoH* in BT-based LOHC systems will also be quantitatively investigated. Furthermore, the proposed methodology will be tested during an ongoing hydrogenation and dehydrogenation reaction inside a reactor for the real-time monitoring of the *DoH*.

Funding sources

This work was funded by the Bavarian Ministry of Economic Affairs, Regional Development and Energy.

Supporting information

The supporting information document for this paper contains the model parameter for the fitted H0-iso- BT and H12-iso-BT spectra in the IHM evaluation.

CRediT authorship contribution statement

Julius H. Jander: Writing – original draft, Investigation, Conceptualization. **Michael H. Rausch:** Writing – review & editing. **Peter Wasserscheid:** Writing – review & editing. **Andreas P. Fröba:** Writing – review & editing, Supervision, Conceptualization.

Declaration of competing interest

The authors declare that they have no known competing financial interests or personal relationships that could have appeared to influence the work reported in this paper.

Achnowledgements

The authors gratefully acknowledge funding of the Erlangen Graduate School in Advanced Optical Technologies (SAOT) by the Bavarian State Ministry for Science and Art.

Appendix A. Supplementary data

Supplementary data to this article can be found online at https://doi.org/10.1016/j.ijhydene.2024.06.357.

References

[1] Faye O, Szpunar J, Eduok U. A critical review on the current technologies for the generation, storage, and transportation of hydrogen. Int J Hydrogen Energy 2022; 47:13771–802. https://doi.org/10.1016/j.ijhydene.2022.02.112.
[2] Durbin DJ, Malardier-Jugroot C. Review of hydrogen storage techniques for on board vehicle applications. Int J Hydrogen Energy 2013;38:14595–617. https://doi.org/10.1016/j.ijhydene.2013.07.058.
[3] Samantaray SS, Putnam ST, Stadie NP. Volumetrics of hydrogen storage by physical adsorption. Inorganics 2021;9:45. https://doi.org/10.3390/inorganics9060045.
[4] Mananghaya MR. Titanium-decorated boron nitride nanotubes for hydrogen storage: a multiscale theoretical investigation. Nanoscale 2019;11:16052–62. https://doi.org/10.1039/C9NR04578C.
[5] Stetson N, Wieliczko M. Hydrogen technologies for energy storage: a perspective. MRS Energy Sustain 2020;7:41. https://doi.org/10.1557/mre.2020.43.

[6] Tarasov BP, Fursikov PV, Volodin AA, Bocharnikov MS, Shimkus YY, Kashin AM, et al. Metal hydride hydrogen storage and compression systems for energy storage technologies. Int J Hydrogen Energy 2021;46:13647–57. https://doi.org/10.1016/j.ijhydene.2020.07.085.
[7] Preuster P, Alekseev A, Wasserscheid P. Hydrogen storage technologies for future energy systems. Annu Rev Chem Biomol Eng 2017;8:445–71. https://doi.org/10.1146/annurev-chembioeng-060816-101334.
[8] Andersson J, Grönkvist S. Large-scale storage of hydrogen. Int J Hydrogen Energy 2019;44:11901–19. https://doi.org/10.1016/j.ijhydene.2019.03.063.
[9] Garcia G, Arriola E, Chen W-H, De Luna MD. A comprehensive review of hydrogen production from methanol thermochemical conversion for sustainability. Energy 2021;217:119384. https://doi.org/10.1016/j.energy.2020.119384.
[10] Moioli E, Schildhauer T. Eco-techno-economic analysis of methanol production from biogas and power-to-X. Ind Eng Chem Res 2022;61:7335–48. https://doi.org/10.1021/acs.iecr.1c04682.
[11] Brückner N, Obesser K, Bösmann A, Teichmann D, Arlt W, Dungs J, et al. Evaluation of industrially applied heat-transfer fluids as liquid organic hydrogen carrier systems. ChemSusChem 2014;7:229–35. https://doi.org/10.1002/cssc.201300426.
[12] Geburtig D, Preuster P, Bösmann A, Müller K, Wasserscheid P. Chemical utilization of hydrogen from fluctuating energy sources – catalytic transfer hydrogenation from charged liquid organic hydrogen carrier systems. Int J Hydrogen Energy 2016;41:1010–7. https://doi.org/10.1016/j.ijhydene.2015.10.013.
[13] Markiewicz M, Zhang YQ, Bösmann A, Brückner N, Thöming J, Wasserscheid P, et al. Environmental and health impact assessment of liquid organic hydrogen carrier (LOHC) systems – challenges and preliminary results. Energy Environ Sci 2015;8:1035–45. https://doi.org/10.1039/C4EE03528C.
[14] Modisha PM, Ouma CNM, Garidzirai R, Wasserscheid P, Bessarabov D. The prospect of hydrogen storage using liquid organic hydrogen carriers. Energy Fuel 2019;33:2778–96. https://doi.org/10.1021/acs.energyfuels.9b00296.
[15] Preuster P, Papp C, Wasserscheid P. Liquid organic hydrogen carriers (LOHCs): toward a hydrogen-free hydrogen economy. Acc Chem Res 2017;50:74–85. https://doi.org/10.1021/acs.accounts.6b00474.
[16] Teichmann D, Arlt W, Wasserscheid P. Liquid Organic Hydrogen Carriers as an efficient vector for the transport and storage of renewable energy. Int J Hydrogen Energy 2012;37:18118–32. https://doi.org/10.1016/j.ijhydene.2012.08.066.
[17] Teichmann D, Arlt W, Wasserscheid P, Freymann R. A future energy supply based on liquid organic hydrogen carriers (LOHC). Energy Environ Sci 2011;4:2767. https://doi.org/10.1039/c1ee01454d.
[18] Jorschick H, Geißelbrecht M, Eßl M, Preuster P, Bösmann A, Wasserscheid P. Benzyltoluene/dibenzyltoluene-based mixtures as suitable liquid organic hydrogen carrier systems for low temperature applications. Int J Hydrogen Energy 2020;45:14897–906. https://doi.org/10.1016/j.ijhydene.2020.03.210.
[19] Kerscher M, Jander JH, Cui J, Maurer LA, Wolf P, Hofmann JD, et al. Thermophysical properties of the liquid organic hydrogen carrier system based on benzyltoluene considering influences of isomerism and dissolved hydrogen. Int J Hydrog Energy 2024;77:1009–25. https://doi.org/10.1016/j.ijhydene.2024.06.131.
[20] Müller K, Aslam R, Fischer A, Stark K, Wasserscheid P, Arlt W. Experimental assessment of the degree of hydrogen loading for the dibenzyl toluene based LOHC system. Int J Hydrogen Energy 2016;41:22097–103. https://doi.org/10.1016/j.ijhydene.2016.09.196.
[21] Aslam R, Khan MH, Ishaq M, Müller K. Thermophysical studies of dibenzyltoluene and its partially and fully hydrogenated derivatives. J Chem Eng Data 2018;63:4580–7. https://doi.org/10.1021/acs.jced.8b00652.
[22] Kerscher M, Klein T, Schulz PS, Veroutis E, Dürr S, Preuster P, et al. Thermophysical properties of diphenylmethane and dicyclohexylmethane as a reference liquid organic hydrogen carrier system from experiments and molecular simulations. Int J Hydrogen Energy 2020;45:28903–19. https://doi.org/10.1016/j.ijhydene.2020.07.261.
[23] Jander JH, Schmidt PS, Giraudet C, Wasserscheid P, Rausch MH, Fröba AP. Hydrogen solubility, interfacial tension, and density of the liquid organic hydrogen carrier system diphenylmethane/dicyclohexylmethane. Int J Hydrogen Energy 2021;46:19446–66. https://doi.org/10.1016/j.ijhydene.2021.03.093.
[24] Berger Bioucas FE, Piszko M, Kerscher M, Preuster P, Rausch MH, Koller TM, et al. Thermal conductivity of hydrocarbon liquid organic hydrogen carrier systems: measurement and prediction. J Chem Eng Data 2020;65:5003–17. https://doi.org/10.1021/acs.jced.0c00613.
[25] Amende M, Gleichweit C, Xu T, Höfert O, Koch M, Wasserscheid P, et al. Dicyclohexylmethane as a liquid organic hydrogen carrier: a model study on the dehydrogenation mechanism over Pd(111). Catal Letters 2016;146:851–60. https://doi.org/10.1007/s10562-016-1711-z.
[26] Schmidt PS, Kerscher M, Klein T, Jander JH, Berger Bioucas FE, Rüde T, et al. Effect of the degree of hydrogenation on the viscosity, surface tension, and density of the liquid organic hydrogen carrier system based on diphenylmethane. Int J Hydrogen Energy 2022;47:6111–30. https://doi.org/10.1016/j.ijhydene.2021.11.198.
[27] Müller K, Stark K, Emel'yanenko VN, Varfolomeev MA, Zaitsau DH, Shoifet E, et al. Liquid organic hydrogen carriers: thermophysical and thermochemical studies of benzyl- and dibenzyl-toluene derivatives. Ind Eng Chem Res 2015;54:7967–76. https://doi.org/10.1021/acs.iecr.5b01840.
[28] Modisha PM, Jordaan JHL, Bösmann A, Wasserscheid P, Bessarabov D. Analysis of reaction mixtures of perhydro-dibenzyltoluene using two-dimensional gas chromatography and single quadrupole gas chromatography. Int J Hydrogen Energy 2018;43:5620–36. https://doi.org/10.1016/j.ijhydene.2018.02.005.
[29] Do G, Preuster P, Aslam R, Bösmann A, Müller K, Arlt W, et al. Hydrogenation of the liquid organic hydrogen carrier compound dibenzyltoluene-reaction pathway determination by ^{1}H NMR spectroscopy. React Chem Eng 2016;1:313–20. https://doi.org/10.1039/c5re00080g.
[30] Dürr S, Zilm S, Geißelbrecht M, Müller K, Preuster P, Bösmann A, et al. Experimental determination of the hydrogenation/dehydrogenation - equilibrium of the LOHC system H0/H18-dibenzyltoluene. Int J Hydrogen Energy 2021;46:32583–94. https://doi.org/10.1016/j.ijhydene.2021.07.119.
[31] Inhetveen P, Alt NSA, Schluecker E. Measurement of the hydrogenation level of dibenzyltoluene in an innovative energy storage system. Vib Spectrosc 2016;83:85–93. https://doi.org/10.1016/j.vibspec.2016.01.008.
[32] Jander JH, Kerscher M, Li S, Rausch MH, Wasserscheid P, Fröba AP. Determination of hydrogen loading in the carrier system diphenylmethane/dicyclohexylmethane by depolarized Raman spectroscopy. Int J Hydrogen Energy 2022;47:9331–45. https://doi.org/10.1016/j.ijhydene.2022.01.005.
[33] Jorschick H, Preuster P, Dürr S, Seidel A, Müller K, Bösmann A, et al. Hydrogen storage using a hot pressure swing reactor. Energy Environ Sci 2017;10:1652–9. https://doi.org/10.1039/c7ee00476a.
[34] Cui J, Kerscher M, Jander JH, Rüde T, Schulz PS, Wasserscheid P, et al. Viscosity and surface tension of fluorene and perhydrofluorene close to 0.1 MPa up to 573 K. J Chem Eng Data 2022;67:3085–96. https://doi.org/10.1021/acs.jced.2c00519.
[35] Jander JH, Piszko M, Kühl JVW, Rausch MH, Fröba AP. Solubility and liquid density of binary mixtures of *n*-hexane or 1-hexanol with krypton, sulfur hexafluoride, or R143a. J Chem Eng Data 2023;68:813–34. https://doi.org/10.1021/acs.jced.2c00727.
[36] Kerscher M, Jander JH, Luther F, Schühle P, Richter M, Rausch MH, et al. Thermophysical properties of the energy carrier methanol under the influence of dissolved hydrogen. Int J Hydrogen Energy 2023;48:26817–39. https://doi.org/10.1016/j.ijhydene.2023.03.312.
[37] Mishra T, De AK, Chattopadhyay S, Mallick PK, Sett P. Electronic and vibrational spectra of diphenylmethane. Spectrochim Acta Part A Mol Biomol Spectrosc 2005;61:767–76. https://doi.org/10.1016/j.saa.2004.02.036.
[38] Barnes RJ, Dhanoa MS, Lister SJ. Standard normal variate transformation and de-trending of near-infrared diffuse reflectance spectra. Appl Spectrosc 1989;43:772–7. https://doi.org/10.1366/0003702894202201.
[39] Mazet V, Carteret C, Brie D, Idier J, Humbert B. Background removal from spectra by designing and minimising a non-quadratic cost function. Chemom Intell Lab Syst 2005;76:121–33. https://doi.org/10.1016/j.chemolab.2004.10.003.
[40] The MathWorks Inc. Optimization Toolbox version 9.5 (R2023a). 2023.
[41] Baglin FG, Whang CM. A Raman spectroscopic study of a vibration-vibration near resonant energy transfer mechanism in liquid toluene-*d*5. J Raman Spectrosc 1976;5:93–9. https://doi.org/10.1002/jrs.1250050111.
[42] Alsmeyer F, Marquardt W. Automatic generation of peak-shaped models. Appl Spectrosc 2004;58:986–94. https://doi.org/10.1366/0003702041655421.
[43] Alsmeyer F, Koß H-J, Marquardt W. Indirect spectral hard modeling for the analysis of reactive and interacting mixtures. Appl Spectrosc 2004;58:975–85. https://doi.org/10.1366/0003702041655368.
[44] Kriesten E, Alsmeyer F, Bardow A, Marquardt W. Fully automated indirect hard modeling of mixture spectra. Chemom Intell Lab Syst 2008;91:181–93. https://doi.org/10.1016/j.chemolab.2007.11.004.
[45] Kriesten E, Mayer D, Alsmeyer F, Minnich CB, Greiner L, Marquardt W. Identification of unknown pure component spectra by indirect hard modeling. Chemom Intell Lab Syst 2008;93:108–19. https://doi.org/10.1016/j.chemolab.2008.05.002.
[46] Hrovat Mirko. Baseline fit (version januar 2009). https://de.mathworks.com/matlabcentral/fileexchange/24916-baseline-fit?focused=5133659&tab=function; 2009.
[47] Bruce SD, Higinbotham J, Marshall I, Beswick PH. An analytical derivation of a popular approximation of the Voigt function for quantification of NMR spectra. J Magn Reson 2000;142:57–63. https://doi.org/10.1006/jmre.1999.1911.
[48] Humlíček J. Optimized computation of the Voigt and complex probability functions. J Quant Spectrosc Radiat Transf 1982;27:437–44. https://doi.org/10.1016/0022-4073(82)90078-4.
[49] Rüde T, Dürr S, Preuster P, Wolf M, Wasserscheid P. Benzyltoluene/perhydro benzyltoluene – pushing the performance limits of pure hydrocarbon liquid organic hydrogen carrier (LOHC) systems. Sustain Energy Fuels 2022;6:1541–53. https://doi.org/10.1039/D1SE01767E.
[50] Giraudet C, Papavasileiou KD, Rausch MH, Chen J, Kalantar A, van der Laan GP, et al. Characterization of water solubility in *n*-octacosane using Raman spectroscopy. J Phys Chem B 2017;121:10665–73. https://doi.org/10.1021/acs.jpcb.7b07580.
[51] Wu W, Klein T, Kerscher M, Rausch MH, Koller TM, Giraudet C, et al. Mutual and thermal diffusivities as well as fluid-phase equilibria of mixtures of 1-hexanol and carbon dioxide. J Phys Chem B 2020;124:2482–94. https://doi.org/10.1021/acs.jpcb.0c00646.
[52] Braeuer A, Knauer OS, Quiño J, Leipertz A. Quantification of the mass transport in a two phase binary system at elevated pressures applying Raman spectroscopy: pendant liquid solvent drop in a supercritical carbon dioxide environment. Int J Heat Mass Transf 2013;62:729–40. https://doi.org/10.1016/j.ijheatmasstransfer.2013.03.046.